Acta Metall. Sin. (Engl. Lett.), 2016, **29**(1), 58–71
DOI 10.1007/s40195-015-0362-1

Effects of Nano-Y_2O_3 and Sintering Parameters on the Fabrication of PM Duplex and Ferritic Stainless Steels

R. Shashanka[1] · **D. Chaira**[1]

Received: 12 August 2015 / Revised: 9 November 2015 / Published online: 4 January 2016

Abstract Here we report the effects of nano-Y_2O_3 addition, sintering atmosphere and time during on the fabrication of PM duplex and ferritic stainless steels composites by dual-drive planetary milling of elemental Fe, Cr and Ni powders followed by conventional pressureless sintering. Yttria-free and yttria-dispersed duplex and ferritic stainless steels are fabricated by conventional sintering at 1000, 1200 and 1400 °C temperatures under argon atmosphere. In another set of experiment, yttria-free and yttria-dispersed duplex and ferritic stainless steels are consolidated at 1000 °C for 1 h under nitrogen atmosphere to study the effect of sintering atmosphere. It has been found that densities of duplex and yttria-dispersed duplex stainless steel increase from 71% to 91% and 78% to 94%, respectively, with the increase in sintering temperature. Similarly, hardness value increases from 257 to 567 HV_{25} in case of duplex, and from 332 to 576 HV_{25} in yttria-dispersed duplex stainless steel. X-ray diffraction analysis shows the domination of more intense austenite phase than ferrite at higher sintering temperature and also in nitrogen atmosphere. It is also evident that addition of yttria enhances phase transformation from α-Fe to γ-Fe. Duplex and yttria-dispersed duplex stainless steels exhibit the maximum compressive yield strength of 360 and 312 MPa, respectively.

KEY WORDS: **Nano-Y_2O_3; Composites; Stainless steel; Powder metallurgy (PM); Mechanical properties; Microstructure; Phase transitions**

1 Introduction

Duplex stainless steel is one of the very important grades of the stainless steel that manifests the properties of both the austenitic and the ferritic stainless steels. Generally, duplex stainless steel contains almost equal proportions of the austenite and the ferrite, but it may vary depending upon the methods of preparation, composition, experimental conditions, etc. This blending effect imparts excellent corrosion resistance, high strength, good weldability, low thermal expansion, high energy absorption, good high-temperature tensile and creep strength [1]. The presence of interstitial atoms and inter-metallic phases impart more strength to duplex stainless steel which acts as obstacles for dislocation motion [2, 3]. Wang et al. [4], Shashanka et al. [5], Miyamoto et al. [6] and Liang et al. [7] reported the superior properties of duplex stainless steel and highlighted its applications in chemical, marine, nuclear power, oil, petrochemical, paper and pulp industries. On the other hand, the ferritic stainless steel is another important grade of the stainless steel having body-centered cubic lattice structure containing less amount of expensive Ni. Dobrzanski et al. [8] and Li et al. [9] reported some excellent properties of the ferritic stainless steel such as high thermal conductivity, less stress corrosion, excellent high temperature oxidation resistance, creep resistance,

Available online at http://link.springer.com/journal/40195

✉ R. Shashanka
shashankaic@gmail.com

[1] Department of Metallurgical and Materials Engineering, National Institute of Technology, Rourkela 769008, India

low thermal expansion, magnetic property and high yield strength. Therefore, it is mainly used in refrigeration cabinets, cold water tanks, chemical and food processing, water treatment plants, street furniture, electrical cabinets, sticking memos on the fridge, storing knives and other metallic implements [4]. Duplex and ferritic stainless steels have wide range of applications; therefore, many researchers are trying to improve their structure and properties by bringing down their microstructure to nano-level and by adding metal oxide dispersing agents.

Planetary milling [10] is one of the most widely used plastic deformation method and used to refine the structure of materials to nano-level. One of the advantages of planetary milling is the production of extremely refined materials in bulk amount at preferably shorter time and with reduced possibility of oxidation. Therefore, we have prepared duplex (Fe–18Cr–13Ni) and ferritic (Fe–17Cr–1Ni) stainless steel powders from their elemental compositions by planetary milling route using specially designed dual-drive planetary mill (DDPM). The mill design, fabrication and the fast, efficient powder synthesis was reported by the authors in their previous paper [11].

In the present work, nano-structured duplex and ferritic stainless steels were prepared by planetary milling and metal oxide dispersoids were further added to improve their mechanical properties [12]. Liu and Li [13], Felten [14], Wukusick and Collins [15] and Francis et al. [16] investigated the effect of oxygen active dispersoids such as nano-Y_2O_3 which imparts strength to interfacial bonding, hinders grain growth and increases hardness of stainless steels.

Sintering atmosphere is one of the most important parameters which involves dew point of the gas and also influences the densification process of the stainless steels to a greater extent [17, 18]. Therefore, we performed sintering of yttria-dispersed and yttria-free stainless steel samples by conventional sintering method in argon and nitrogen atmospheres at 1000 °C for 1 h. Kurgan reported the effect of sintering atmosphere (argon and nitrogen) on the AISI 316L stainless steel compacts. He studied the sintered density, grain morphology and mechanical properties of AISI 316L stainless steel sintered at argon and nitrogen atmospheres, and concluded that the AISI 316L compacts sintered in nitrogen atmosphere exhibit higher strength and hardness than the steels sintered in argon atmosphere [19]. Martin et al. [20] consolidated duplex stainless steel at 650 and 700 MPa in nitrogen and hydrogen atmospheres at a temperature of 1250 °C. The sintering of compacted duplex stainless steel was carried out for 30, 60, 120 and 240 min, respectively, and at different cooling rates (furnace, gas and water cooling) to study the microstructure and mechanical properties. They reported that furnace-cooled duplex stainless steel samples exhibit a high tensile strength than the base materials and water-cooled duplex stainless steels. They concluded that water cooling can increase the hardness of duplex stainless steel, but it decreases the tensile strength and ductility. Pandya et al. [21] reported the densification process of the austenitic stainless steel at 1200, 1300 and 1400 °C, respectively, and studied the effect of sintering temperature on the microstructure and mechanical properties of austenitic stainless steel. They correlated processing parameters, microstructure and properties and concluded that the density of the austenitic stainless steel increases with the increase in sintering temperature. Vijayalakshmi et al. [22] investigated the microstructural evolution and mechanical properties of duplex stainless steel at 1100, 1200, 1300 and 1350 °C sintering temperatures. They correlated microstructural changes at different temperatures and concluded that the surface hardness mainly depends upon the phases present in the materials. Shashanka and Chaira [23] prepared nano-structured duplex and the ferritic stainless steel powders by Pulverisette planetary milling of elemental Fe, Cr and Ni powder for 40 h. They consolidated both the stainless steels by conventional pressureless sintering at 1000, 1200 and 1400 °C temperatures, respectively, in argon atmosphere to study the microstructure, density and hardness. They achieved 90% of sintered density and 550 HV Vickers microhardness for duplex stainless steel sintered at 1400 °C for 1 h. Similarly, they achieved 92% sintered density and 263 HV microhardness for the ferritic stainless steel sintered at 1400 °C. Shashanka and Chaira [11] synthesized duplex and ferritic stainless steels in a very fast and efficient manner by planetary milling of elemental powders in dual-drive planetary mill (DDPM). They reported that only 10 h of milling is sufficient to prepare more than 500 g of nano-structured stainless steel powders using DDPM, whereas other conventional planetary millings can produce only few grams in more than 20 h and hence they concluded that DDPM method of stainless steel preparation is fast and efficient.

In the present investigation, our aim is to study the effect of nano-Y_2O_3, sintering atmosphere and time during synthesis of nano-structured duplex and ferritic stainless steels by planetary milling followed by conventional sintering. Here, we also investigate the microstructural evolution, mechanical properties and phase transformation of yttria-dispersed and yttria-free duplex and ferritic stainless steels during milling and consolidation. Microstructure, density and hardness values of all the stainless steel samples fabricated by conventional sintering method in argon and nitrogen atmospheres at 1000 °C are compared. The effect of nano yttria addition is also studied successfully.

2 Experimental

The detailed study of synthesis of duplex (Fe–18Cr–13Ni) and ferritic stainless steel (Fe–17Cr–1Ni) powder by dual-drive planetary milling was explained by authors in their previous papers [24, 25]. Carbon content of the both 10-h milled stainless steel powders were measured by CHNS analyzer (Elementar Analysensysteme, Germany/Vario EL). Planetary-milled stainless steel powders were mixed separately with 1 wt% nano-Y_2O_3 powder particles in a turbula shaker mixer (TURBULA® T2F, Willy A. Bachofen AG Maschinenfabrik, Switzerland) for 3 h. Yttria-dispersed and yttria-free duplex and ferritic stainless steel powder samples were consolidated by pressureless conventional sintering method.

All the stainless steel samples were compacted using hydraulic press at 700 MPa and polyvinyl alcohol as binder. Compacted stainless steel samples were conventionally sintered at 1000, 1200 and 1400 °C, respectively, in a tubular furnace with holding time of 1 h each under argon atmosphere to study the effect of temperature. In a separate set of experiment, conventional sintering was carried out at 1000 °C under nitrogen atmosphere for 1 h to study the effect of sintering atmosphere.

All the stainless steel samples were polished carefully for microscopic investigation. The density and microhardness values were measured by Archimedes method [26] and Vickers microhardness methods, respectively. Vickers microhardness studies were carried out using LECO-LM248AT fitted with a Vickers pyramidal diamond intender. Carl Zeiss optical microscope was used to study the microstructure of consolidated stainless steel samples, and their phase fraction was calculated by using Axio Vision Release 4.8.2 SP3 (08-2013) software. The consolidated stainless steel samples were characterized by X-ray diffraction (XRD) in a Philips PANalytical diffractometer using filtered CuK_α-radiation ($\lambda = 0.1542$ nm). Compression tests were performed in an Instron corporation series IX automated Materials testing 1.26 systems at room temperature and at a strain rate of 1 mm/min. All the yttria-dispersed and yttria-free duplex and ferritic stainless steel specimens have the cylindrical disk-shaped structure with an average *H*/*D* ratio of 1.10.

3 Results and Discussion

3.1 Synthesis and Characterization of Milled Duplex and Ferritic Stainless Steel Powder

The elemental powder mixture of Fe, Cr and Ni of composition Fe–18Cr–13Ni (duplex) and that of composition Fe–17Cr–1Ni (ferrite) were selected from Schaeffler diagram. The above compositions were milled in a specially designed DDPM for 10 h with 6:1 ball to powder weight ratio under toluene atmosphere to prevent oxidation. Figure 1a and b shows the microstructure of duplex and ferritic stainless steel powders after 10 h of milling. The detailed study of microstructural evolution of duplex and ferritic stainless steel powders was explained by the authors in their previous publications [11, 23, 24]. The 10-h milled stainless steel powders exhibit regular, small and spherical shapes as shown in the SEM microstructures. We studied the qualitative and quantitative analyses of 10-h milled duplex and the ferritic stainless steel powders by EDS as shown in Fig. 1c, d, respectively. The EDS analysis confirms the homogeneous distribution of elements with almost same composition as that of initial parental elemental composition. The amount of carbon present in the 10-h milled stainless steel samples were measured by using CHNS analyzer. It was found that duplex stainless steel contains 0.077% of carbon, whereas ferritic stainless steel contains 0.093% of carbon. Figure 2 depicts the FESEM image of as-received Y_2O_3 nanoparticles. The yttria nanoparticles are regular and spherical shape with an average particle size of around 40 nm.

3.2 Consolidation of Duplex and Ferritic Stainless Steel Powders

3.2.1 Effect of Sintering Temperature

3.2.1.1 Phase Analysis by XRD The XRD spectra of duplex and ferritic stainless steel samples sintered at 1000, 1200 and 1400 °C are shown in Fig. 3a, b, respectively. The XRD spectra of conventionally consolidated duplex and ferritic stainless steel samples show sharp and crystalline diffraction peaks of the ferrite and the austenite phases. The sharpness and crystallinity of diffraction peaks increase with the increase in sintering temperature from 1000 to 1400 °C. During milling, the stainless steel powder has undergone many transformations like introduction of structural defects, amorphization, reduction in crystallite size and the increase in volume fraction of grain boundaries. This increases the number of defect storage sites, shortens diffusion paths and attains non-equilibrium state [27]. But during sintering, the stainless steel powder particles diffuse and rearrange themselves in a regular manner, and this increases the crystallinity of stainless steel. The rate of diffusion, grain growth and the atomic periodicity increases with the increase in sintering temperature. Figure 3c and d depicts the XRD spectra of conventionally sintered yttria-dispersed duplex and ferritic stainless steel samples at 1000, 1200 and 1400 °C, respectively. Both stainless steel samples show high intense, sharp crystalline

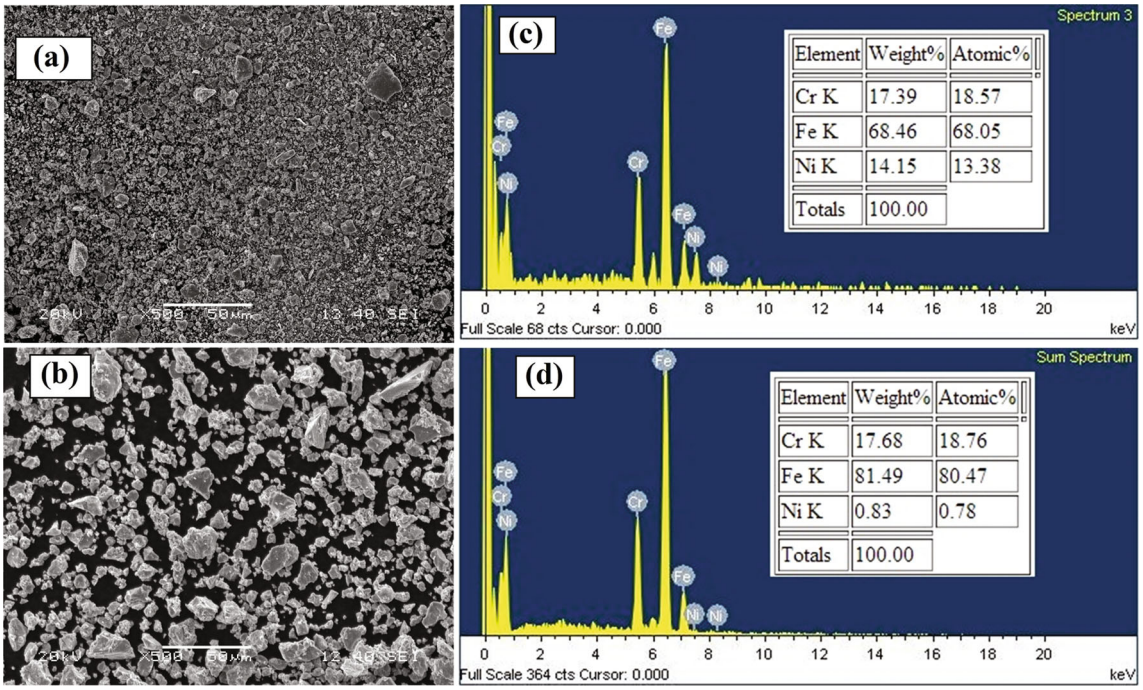

Fig. 1 SEM images of duplex **a** and **f**erritic **b** stainless steel milled for 10 h; similarly EDS of duplex **c** and ferritic **d** stainless steel powders milled for 10 h in DDPM

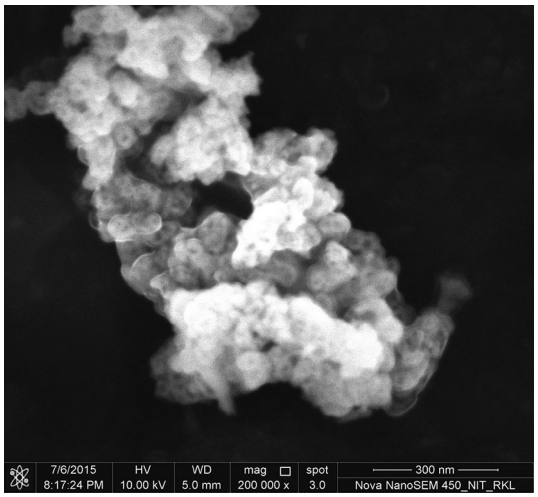

Fig. 2 FESEM microstructure of as-received Y_2O_3 nanoparticles

diffraction peaks as shown in the figures. The yttria-dispersed duplex stainless steel shows phase transformation from α-Fe to γ-Fe during sintering and results in more dominant austenite phase at higher temperature. Figure 3c clearly shows the phase transformation of α-Fe to γ-Fe by resolving both austenite and ferrite peaks at 1000 °C. The intensity and percentage volume of the austenite phase increase with the increase in sintering temperature. At 1400 °C, the austenite peaks become more dominant than ferrite peaks in case of yttria-dispersed duplex stainless steel. The yttria-dispersed duplex stainless steel shows more intense and predominant austenite peaks than the yttria-free duplex stainless steel where phase transformation is limited even at higher temperature. The phase transformation is due to the dispersion of Y_2O_3 in stainless steel. The phase transformation may be due to the diffusion of yttria atoms into the smaller interstitial sites of ferrite crystallites, forms mismatch strains and thus initiates phase transformation [11]. The refinement of ferrite crystallite to nano-level can also initiate phase transformation. Therefore, more research work is to be carried out to study the mechanism of yttria during austenitic stabilization. Both the XRD spectra show no sigma phases, carbides or nitride precipitations of secondary phases.

3.2.1.2 Microstructure and Phase Analysis Figure 4a and b shows the optical micrographs of duplex and ferritic stainless steel samples consolidated at 1000, 1200 and 1400 °C, respectively. From the microstructures, it is confirmed that the number of the pores decreases with the increase in sintering temperature from 1000 to 1400 °C. This is due to rapid rate of mass transport at higher temperatures through necking. At 1400 °C, material dissolution takes place primarily at the interior of both the stainless steel samples. At 1400 °C, the part of very fine stainless steel powders melts and forms pendular bonds at their particle contacts. Due to weak and semisolid bonding between the particles decreases the viscosity of the liquid.

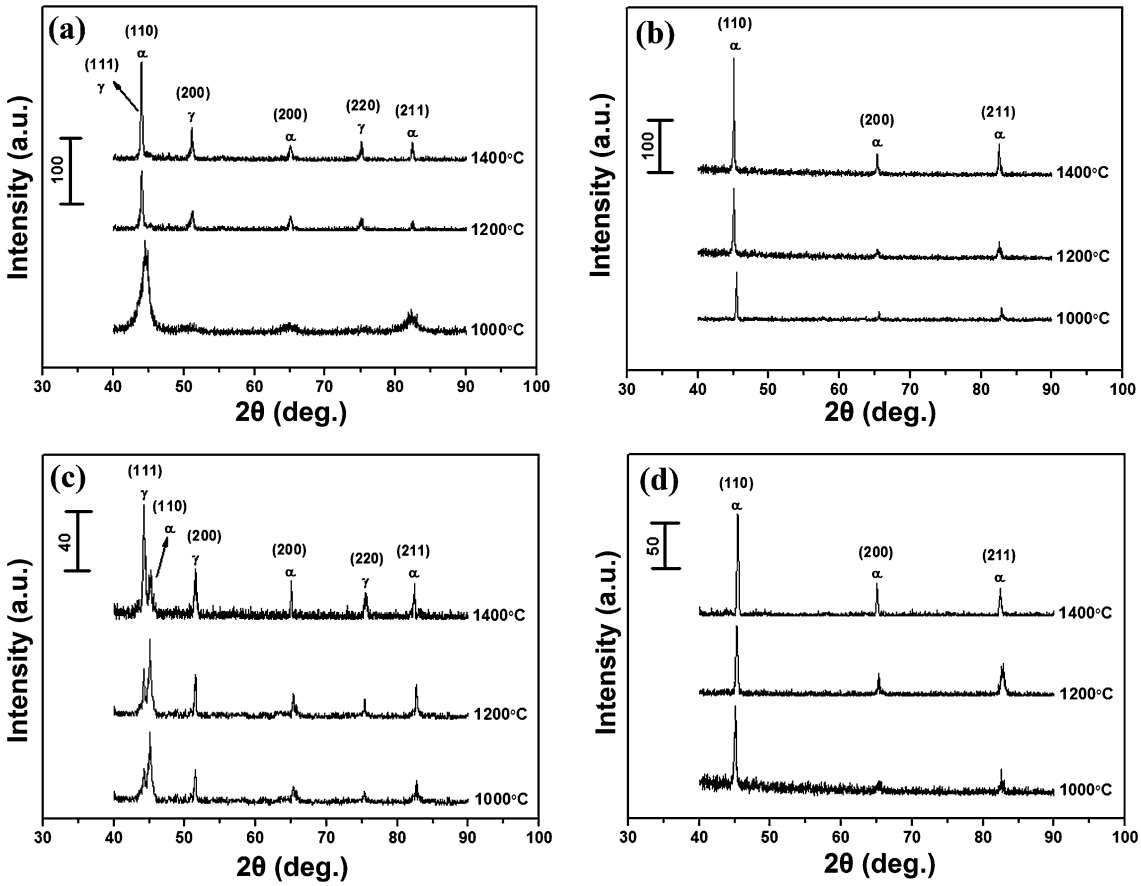

Fig. 3 XRD spectra of duplex **a**, ferritic **b** stainless steel, yttria-dispersed duplex **c** and yttria-dispersed ferritic **d** stainless steel samples sintered at 1000, 1200 and 1400 °C in argon atmosphere

Then low viscous liquid flows freely through capillary action and results in rapid viscous flow sintering densification [28–30]. Therefore, the stainless steel sintered at 1400 °C exhibits low porosity ratio, high density and maximum hardness. Pandya et al. [21] also reported similar results of material dissolution at 1400 °C. Figure 4c, d represents the optical micrographs of yttria-dispersed duplex and ferritic stainless steel samples sintered at 1000, 1200 and 1400 °C, respectively. The increase in sintering temperature from 1000 to 1400 °C decreases the number of the pores and increases the density of sample as well as the fraction of austenite phase in both the stainless steels, as shown in Fig. 4. Therefore, we have carried out an investigation to study the extent of volume fraction of the ferrite and the austenite phase formed in both yttria-dispersed and yttria-free stainless steel during sintering. The volume fraction of both ferrite and austenite phases are calculated by Axio Vision Release software. The volume fraction of the austenite phase increases from 51 to 65% during sintering from 1000 to 1400 °C in case of duplex and from 57 to 72% in case of yttria-dispersed duplex stainless steel. Similarly, the volume fraction of the austenite phase increases from 33 to 58% in ferritic stainless steel and from 41 to 62% in the yttria-dispersed ferritic stainless steel during sintering from 1000 to 1400 °C. In the micrographs, ferrite (α-white), austenite (γ-gray) and pores (P-black) are shown.

3.2.1.3 Density and Hardness Study Figure 5a represents the effect of sintering temperature on the densities of yttria-free duplex, ferritic stainless steel, yttria-dispersed duplex and ferritic stainless steel samples, respectively. The density of all four stainless steel samples increases with the increase in sintering temperature from 1000 to 1400 °C. At higher temperature, the rate of diffusion is more effective and the atoms rearrange themselves in a very dense pattern. A maximum density of more than 94% is achieved for both yttria-dispersed duplex and ferritic stainless steel samples at 1400 °C sintering temperature. The optical microstructures of yttria-dispersed duplex stainless steel show very less porosity ratio with the increase in sintering temperature. It is observed from the microstructures that the porosity ratio of yttria-dispersed duplex stainless steel is less compared to yttria-free duplex stainless steel. This is

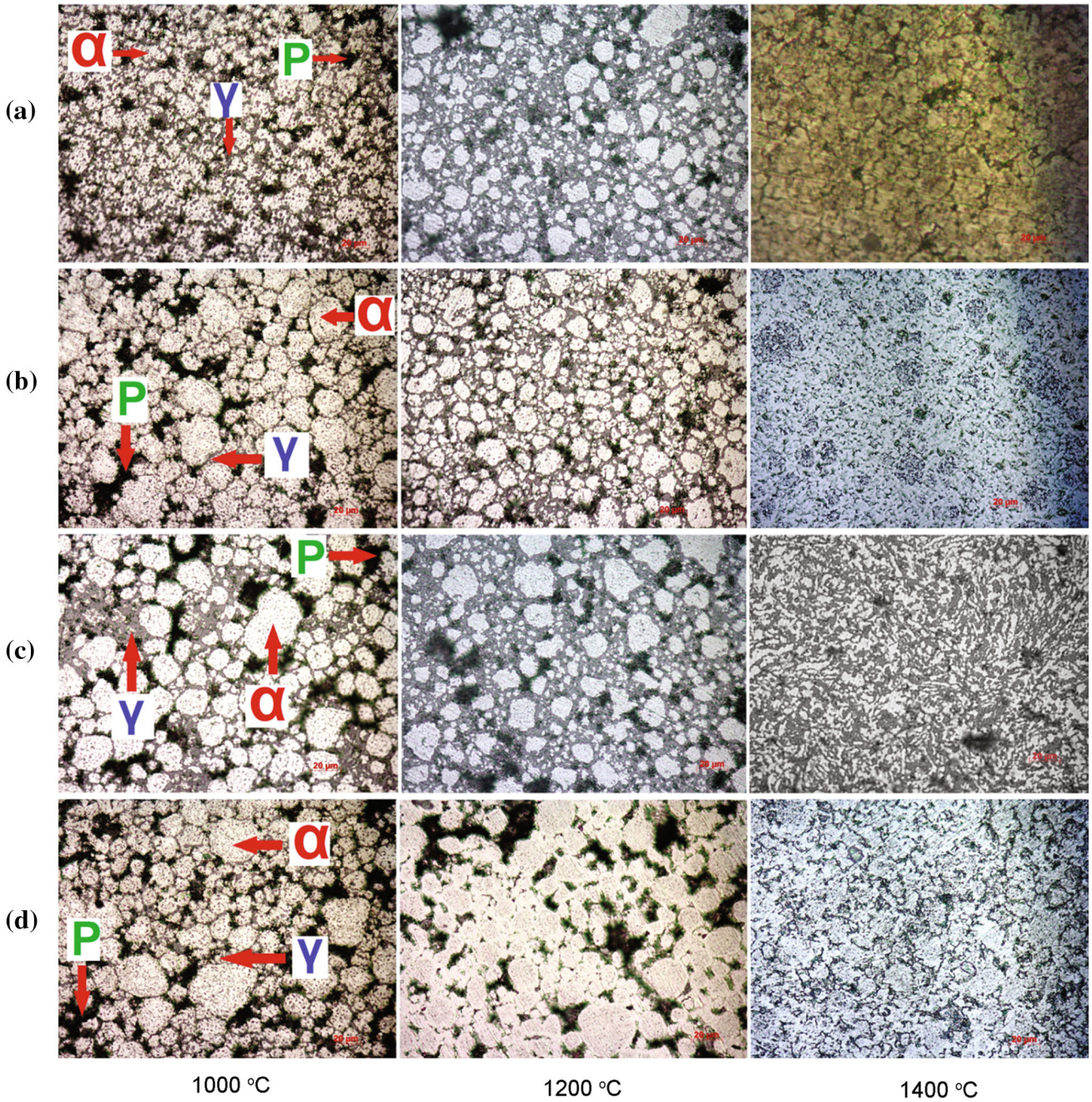

Fig. 4 Optical microstructure of duplex **a**, ferritic **b** stainless steel, yttria-dispersed duplex **c** and yttria-dispersed ferritic **d** stainless steel samples sintered at 1000, 1200 and 1400 °C in argon atmosphere (*P* Pores)

due to the accommodation of yttria nanoparticles in the interstices of micron-sized stainless steel particles and hinders the grain growth. As Tiwari et al. [31] reported, the added yttria nanoparticles have a tendency to increase the propensity for grain boundary added diffusion and the addition of yttrium aluminum garnet (YAG) to ferritic (434L) stainless steel improves the densification, mechanical and tribological properties. They performed sintering at both solid-state (1200 °C) and super-solidus (1400 °C) sintering conditions and concluded that super-solidus sintering and YAG addition result in superior densification and enhancement of the hardness of ferritic stainless steels. They also reported that addition of 10 wt% YAG results in YAG–YAG bonding instead of YAG–stainless steel. This decreases the density and hardness of stainless steel. Therefore, they concluded that addition of small amount of YAG (5 wt%) results in strong YAG–stainless steel bonding [31]. Jain et al. [32] also reported that addition of

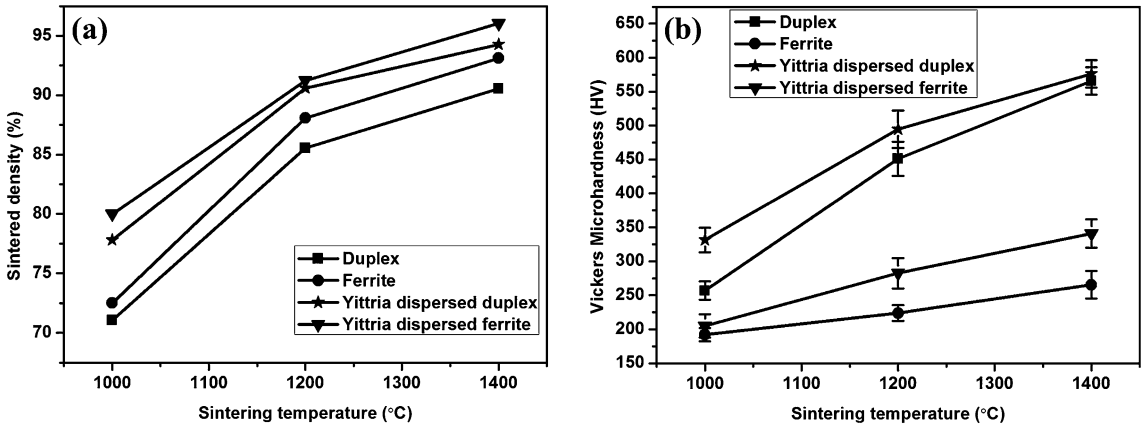

Fig. 5 Curves of sintered density **a** and Vickers microhardness **b** of stainless steel samples sintered at 1000, 1200 and 1400 °C in argon atmosphere

more percentage of yttria nanoparticles increases the possibility of yttria–yttria interaction rather than yttria–stainless steel interaction and agglomerates at grain boundaries and decreases the strength of stainless steel. Optical microstructure of all the stainless steel samples confirms that the increase in sintering temperature decreases the number of pores and increases the density. The density of duplex and ferritic stainless steels varies from 71% to 91% and from 73% to 93%, respectively, at sintering temperature of 1000 to 1400 °C. Similarly, the density of yttria-dispersed duplex and ferritic stainless steels varies from 78% to 94% and from 80% to 96%, respectively.

Figure 5b represents the Vickers microhardness values of yttria-dispersed and yttria-free stainless steel samples measured at 245-mN indentation load. At higher sintering temperature, the density increases due to the less number of voids and hence hardness also increases. The Vickers microhardness value is calculated using the relation [33].

$$HV = 1.8544\frac{P}{d^2} \tag{1}$$

where P is the applied load and d is the diagonal length of the indentation. Yttria-dispersed duplex and ferritic stainless steel samples show more hardness values than yttria-free duplex and ferritic stainless steels, respectively. Addition of yttria in stainless steel increases the bonding strength, density and hinders grain growth. As a result, yttria-dispersed stainless steel exhibits higher hardness than yttria-free stainless steels. The Vickers microhardness values of duplex and ferritic stainless steels change from 257 to 567 HV and 192 to 265 HV, respectively, for variation of sintering temperature from 1000 to 1400 °C. Similarly, the hardness values change from 332 to 576 HV for yttria-dispersed duplex and from 205 to 341 HV for ferritic stainless steel, respectively. Figure 6 depicts the effects of the indentation load on the microhardness of duplex, ferritic, yttria-dispersed duplex and the ferritic stainless steel samples sintered at 1000, 1200 and 1400 °C, respectively. The Vickers microhardness measurements of all the stainless steel samples were carried out at three different loads 98, 245 and 490 mN with a dwell time of 10 s. For each stainless steel sample, at least five trials of the indentations were made at each load and the average values of the diagonal lengths of the indentation marks were measured as hardness. From Fig. 6a–d, it is observed that the hardness values of respective stainless steel sample decrease with the increase in applied indentation load. This is due to the indentation size effect (ISE), and it occurs due to the surface effect and strain gradient effect [23, 34]. ISE also directly relates to the intrinsic structural factors of the tested materials such as indentation elastic recovery, work hardening during indentation and surface dislocation pining [35, 36]. The hardness of the tested specimen is a measure of the indentation depth, which is inversely proportional to hardness [37]. Therefore, with the increase in applied load from 98 to 490 mN, the indentation depth increases and thus decreases the hardness values as shown in the figure. Mott [38], Buckle [39], Gane [40], Upit and Varchenya [41] and Chen et al. [42] reported the significant variations of hardness with depth, especially at depths of less than a few micrometers, and they also reported the possibility of two types of effects. Normal ISE increases the hardness at smaller depths, and reverse ISE decreases the hardness. But in our case due to normal ISE, the hardness decreases with the increase in the indentation depth.

3.2.1.4 Compressive Strength Figure 7 shows the compression yield stresses of the yttria-dispersed, the yttria-free duplex and the ferritic stainless steel samples sintered at 1000 °C. It is shown that yttria-dispersed stainless steel shows maximum resistance to deformation than the yttria-

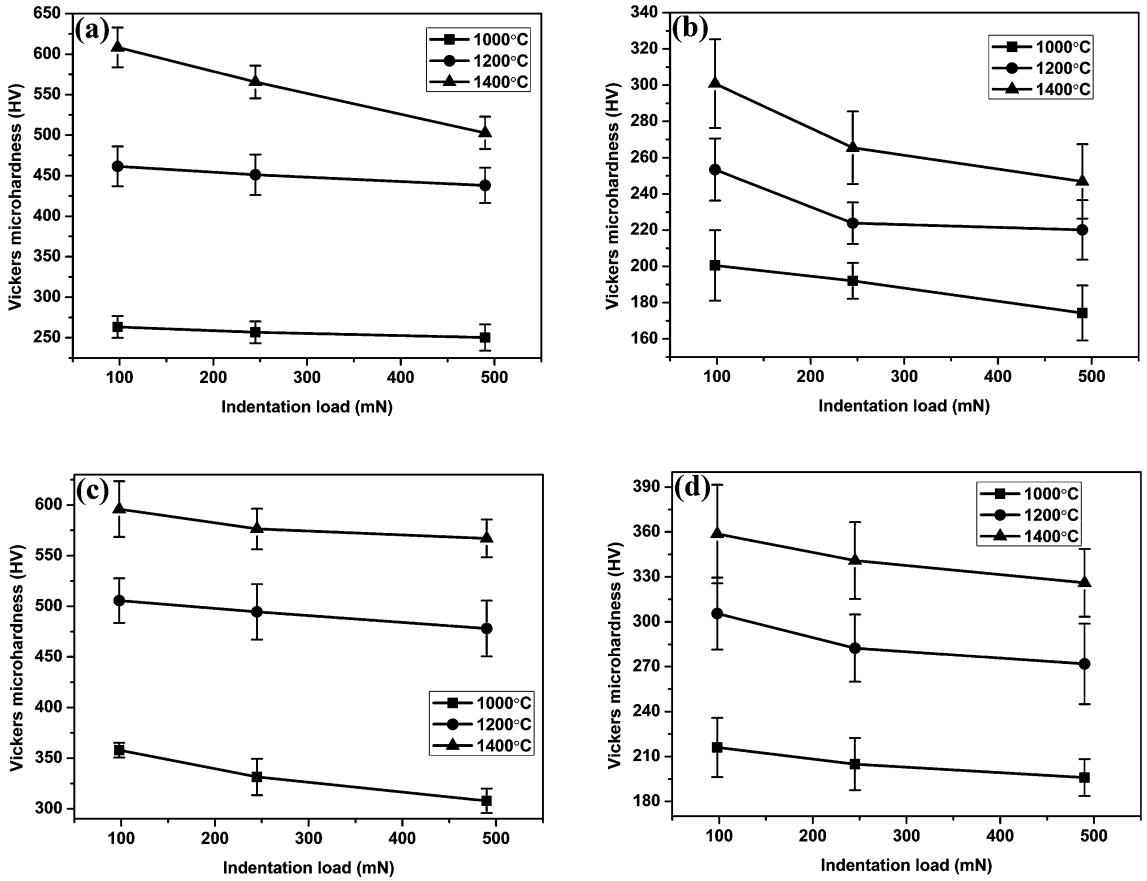

Fig. 6 Effect of indentation load (98, 245 and 490 mN) on Vickers microhardness of duplex **a**, ferritic **b** stainless steel, yttria-dispersed duplex **c** and yttria-dispersed ferritic **d** stainless steel samples sintered at 1000, 1200 and 1400 °C in argon atmosphere

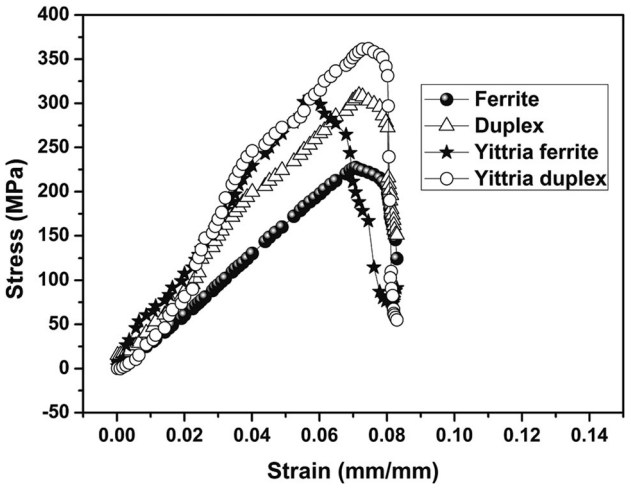

Fig. 7 Compressive stress–strain curves of the yttria-dispersed and yttria-free duplex and ferritic stainless steel samples sintered at 1000 °C in argon atmosphere

free stainless steel. We know that the yttria-dispersed stainless steel exhibits maximum density and hardness values and hence more stress is required to deform them. The addition of yttria increases strengthening, inhibits dislocation motion, increases the deformation resistance, controls the recovery and re-crystallization process and inhibits the grain growth [43]. As a result, the yttria-dispersed stainless steel sintered at 1000 °C shows maximum yield stress than the yttria-free stainless steels. Yttria-dispersed duplex and ferritic stainless steels exhibit the maximum compressive yield stresses of 360 and 308 MPa, respectively, whereas yttria-free duplex and ferritic stainless steels possess maximum yield stresses of 312 and 225 MPa, respectively. The toughness values of duplex and ferritic stainless steels are found to be 24 and 9 MPa, respectively. Similarly, the toughness of yttria-dispersed duplex and yttria-dispersed ferritic stainless steels are found to be 28 and 15 MPa, respectively. The values of the volume fractions, density, hardness and compressive strength of austenite and ferrite phases of yttria-dispersed and yttria-free stainless steel samples sintered in argon atmosphere are tabulated in Table 1. The composition, preparation, processing methods, density, microhardness and yield stress of stainless steels investigated by different authors are tabulated in Table 2.

Table 1 Volume fractions, density and hardness of the austenite and ferrite phases of stainless steel samples sintered in argon atmosphere at different sintering temperature

Sample	Sintering temperature (°C)	Volume fraction (%)		Theoretical density (g/mL)	Sintered density (%)	Vickers microhardness (HV)	Compressive strength (MPa)
		Austenite phase	Ferrite phase				
Duplex stainless steel	1000	51	49	7.84	71.05	257	312
	1200	62	38		85.55	451	
	1400	65	35		90.56	567	
Ferritic stainless steel	1000	33	67	7.75	72.5	192	225
	1200	44	56		88.08	224	
	1400	58	42		93.12	265	
Yttria-dispersed duplex stainless steel	1000	57	43	7.80	77.81	332	360
	1200	65	35		90.6	495	
	1400	72	27		94.28	576	
Yttria-dispersed ferritic stainless steel	1000	41	58	7.70	79.99	205	308
	1200	52	48		91.23	282	
	1400	62	38		96.05	341	

Table 2 Composition, preparation, processing methods, density, microhardness and yield stress of stainless steels investigated by different authors

Reference	Composition	Powder preparation	Processing method	Density (%)	Vickers microhardness (HV)	Yield stress (MPa)
[43]	Ni–20Cr–1.2Y_2O_3	SPEX 8000 M shaker mill for 2 h	SPS at 1100 °C for 30 min	99.55	472	1286
[44]	AISI 304L		Equal channel angular pressing at 700 °C		225	652
[45]	Fe–18Cr–8Mn–0.9 N	High-energy shaker mill for 144 h under nitrogen gas	Conventional sintering at 1100 °C for 30 h	87.3	324	270
[46]	74Fe–18Cr–8Mn	High-energy shaker mill for 120 h under nitrogen gas	Conventional sintering at 1100 °C for 20 h	83.1	495	390
[47]	316L SS	Gas atomization	Direct laser deposition method using 1 kW Nd: YAG laser		215	408
[48]	Fe–17Cr–10Mn–3Mo–0.4Si–0.5 N–0.2C	Planetary ball mill for 48 h under argon gas	Conventional sintering at 1050 °C for 1 h and water quenched			542
[Present paper]	Fe–18Cr–13Ni	Dual-drive planetary mill for 10 h under toluene	Conventional sintering at 1000 °C for 1 h in argon atmosphere	71.05	257	312

3.2.2 Effect of Sintering Atmosphere

3.2.2.1 Phase Analysis by XRD Figure 8a and b represents the XRD spectra of duplex and ferritic stainless steel samples sintered conventionally at 1000 °C in nitrogen atmosphere. Both the stainless steels show sharp and crystalline diffraction peaks. From the XRD graphs, it is confirmed that the austenite peaks are more dominant in duplex stainless steel; and the ferrite peaks are dominant along with austenite and traces of iron nitride phases in ferritic stainless steel, respectively. Ferritic stainless steel sintered in nitrogen atmosphere shows α-Fe to γ-Fe phase transformation, but phase transformation is absent in ferritic stainless steel sintered at argon atmosphere. It is widely accepted that nitrogen favors the α-Fe to γ-Fe phase transformation [11] and therefore sintering atmosphere plays an important role in phase transformation. Limited amount of austenite phase forms during milling, and hence

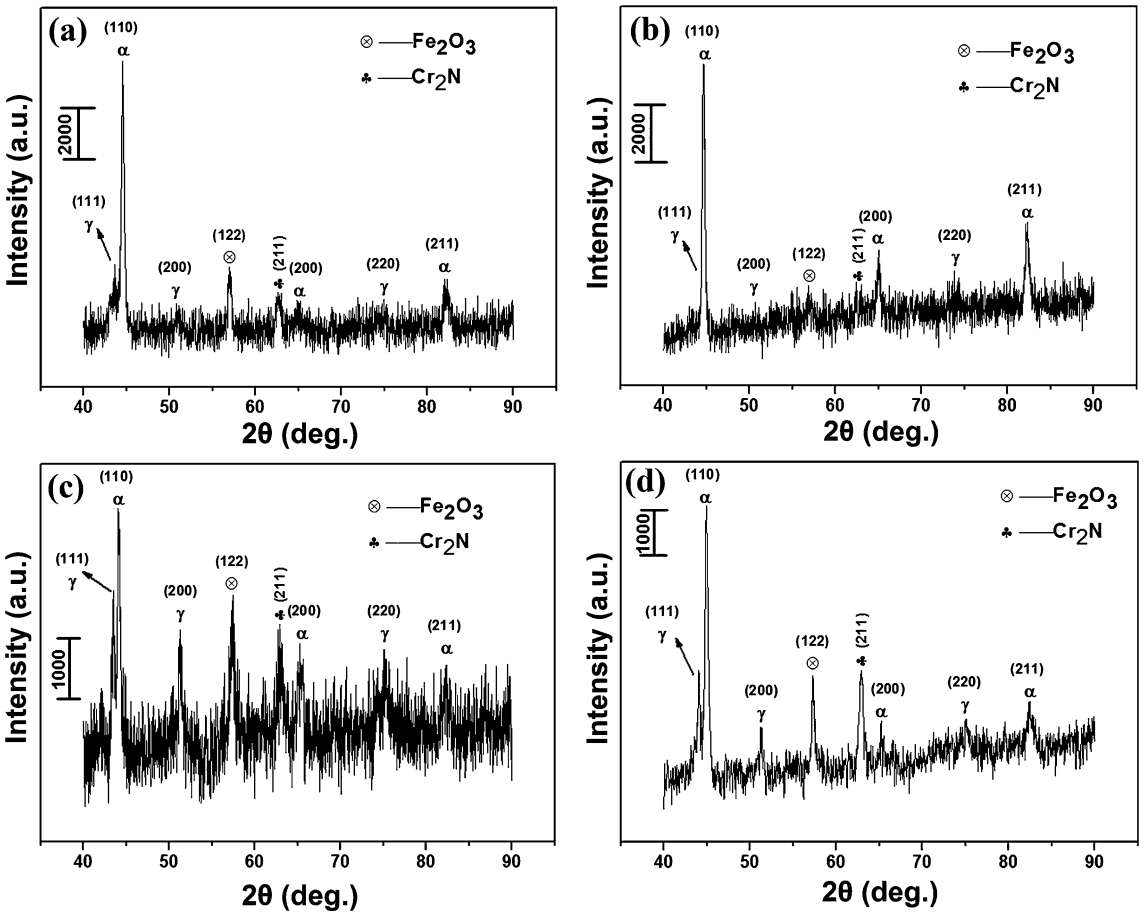

Fig. 8 XRD spectra of duplex **a**, ferritic stainless steel **b**, Yttria-dispersed duplex **c**, Yttria-dispersed ferritic stainless steel **d** samples sintered at 1000 °C in nitrogen atmosphere

sintering of stainless steel compacts can promote α-Fe to γ-Fe. Comparing the diffraction peaks of ferritic stainless steel sintered at 1000 °C in argon and nitrogen atmospheres (Fig. 3 and Fig. 8), we can observe the formation of γ-Fe peaks in ferritic stainless steel sintered in nitrogen atmosphere; but austenite peaks are absent in argon atmosphere sintering. Austenite has large interstitial sites and smaller interfacial energy, whereas ferrite has smaller interstitial sites and larger interfacial energy. During sintering in nitrogen atmosphere, N_2 atoms diffuse into the larger interstitial sites of austenite and form very less distortion and volume mismatch. But in case of ferrite, N_2 atoms diffuse into the smaller interstitial sites and create mismatch strains. The presence of alloying elements such as Cr and Ni in ferritic stainless steel increases the solubility of N_2 atoms in Fe lattice. Ferritic stainless steel contains alloying elements such as Cr and Ni, and they increase the solubility of nitrogen atoms in Fe lattice. During milling, many processes such as introduction of structural defects, distortion of crystallite lattice and refinement in grain size, fracturing and cold welding of powder particles take place. This results in maximum defect storage sites and shorter diffusion paths. Therefore, during sintering, N_2 atoms easily diffuse into Fe lattice through shorter diffusion paths and piled in defect storage sites. The increased ratio of lattice strain to grain size increases the preferable lattice storage sites for nitrogen absorption [49] and thereby enhances the α-Fe to γ-Fe phase transformation. All the above explanation provides more evidence that nitrogen acts as austenitic stabilizer. Figure 8c, d depicts the XRD spectra of yttria-dispersed duplex and ferritic stainless steel samples conventionally sintered at 1000 °C in nitrogen atmosphere. Yttria-dispersed ferritic stainless steel shows a phase transformation from α-Fe to γ-Fe in presence of nitrogen atmosphere. But the phase transformation is absent in case of yttria-dispersed ferritic stainless steel sintered in argon atmosphere at 1000 °C. XRD spectra of all four stainless steel samples sintered at nitrogen atmosphere show secondary iron nitride phase, which enhances the hardness of the material.

3.2.2.2 Microstructure and Phase Analysis Optical micrographs of yttria-dispersed, yttria-free duplex and ferritic stainless steel samples consolidated at 1000 °C in nitrogen atmosphere are shown in Fig. 9. All the microstructures show a low porosity ratio which improves the mechanical properties significantly, whereas stainless steel samples sintered at 1000 °C in argon atmosphere possess a high ratio of porosity with irregular shapes. Stainless steel samples sintered in nitrogen atmosphere form secondary phases such as chromium nitrides at grain boundaries of Fe matrix as shown in the micrographs and forms tri-phase structure. But secondary phases are absent in stainless steel samples sintered in argon atmosphere at 1000 °C (Fig. 4), and they show only bi-phase structure [50]. The presence of chromium nitride phase and phase transformation from α-Fe to γ-Fe has been confirmed by XRD spectra. As we have discussed earlier, nitrogen acts as austenitic stabilizer, and therefore, stainless steel samples sintered in nitrogen atmosphere show more volume fraction of the austenite than the stainless steel sintered in argon atmosphere. Figure 10 represents the volume fraction analysis of yttria-free, yttria-dispersed duplex and ferritic stainless steels, respectively. In the micrographs, ferrite (Blue), austenite (Green) and chromium nitride (Red) are shown. The volume fraction of austenite phase is 63% for duplex and 40% for the ferritic stainless steel sintered in nitrogen atmosphere, whereas the same stainless steel sintered at argon atmosphere shows the contents of austenite phase of 51 and 33 vol%, respectively. Yttria-dispersed duplex and ferritic stainless steel samples sintered at nitrogen atmosphere show the contents of austenite phase of 79 and 45 vol%. Similarly, yttria-dispersed duplex and ferritic stainless steels sintered at argon atmosphere show the contents of austenite phase of 57 and 41 vol%, respectively.

3.2.2.3 Density and Hardness Study Figure 11a represents the effect of sintering atmosphere on the densities of duplex, ferritic and yttria-dispersed duplex and ferritic stainless steel samples, respectively. It is found that conventional sintering carried out under nitrogen atmosphere results in higher values of density and hardness as compared to sintered at argon atmosphere. Kurgan [19] also reported similar kind of results. Optical microstructures of the stainless steel show regular arrangement with low porosity ratio and high density. But the stainless steel

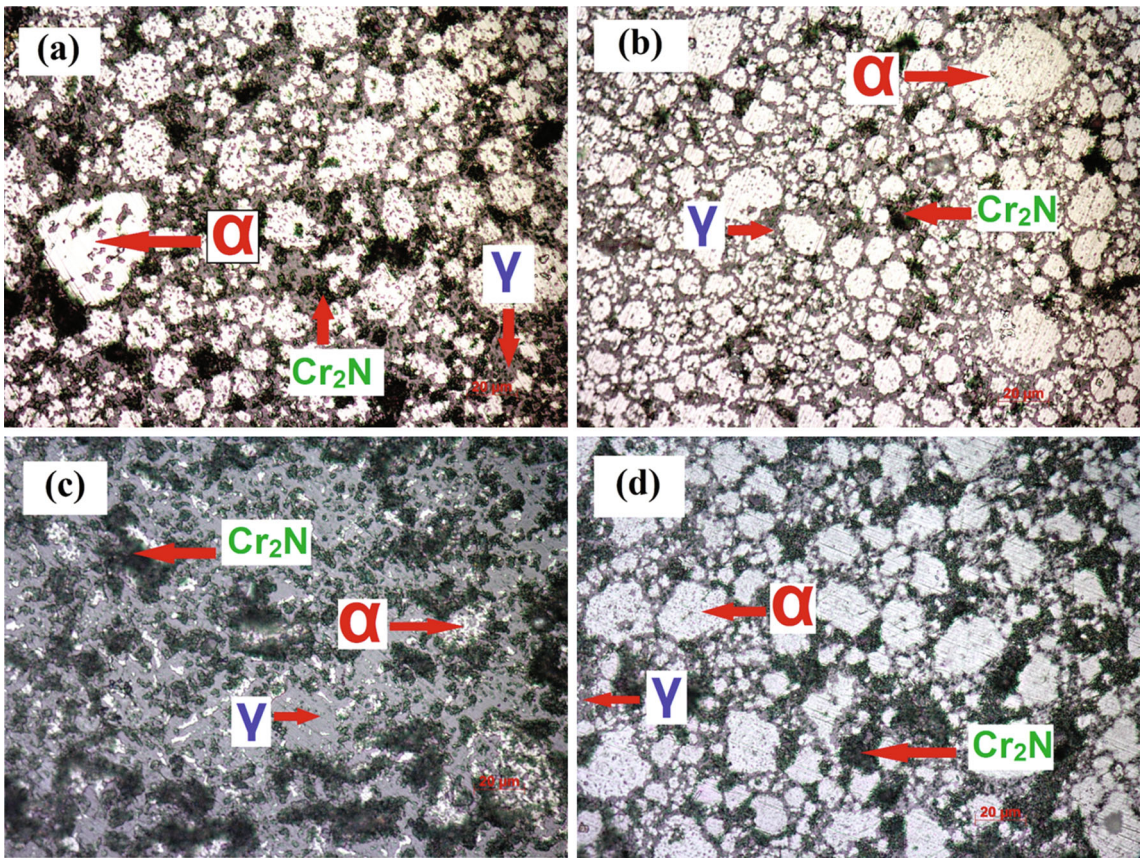

Fig. 9 Optical microstructures of duplex **a**, ferritic stainless steel **b**, yttria-dispersed duplex **c** and yttria-dispersed ferritic stainless steel **d** samples sintered at 1000 °C in nitrogen atmosphere (*P* pores)

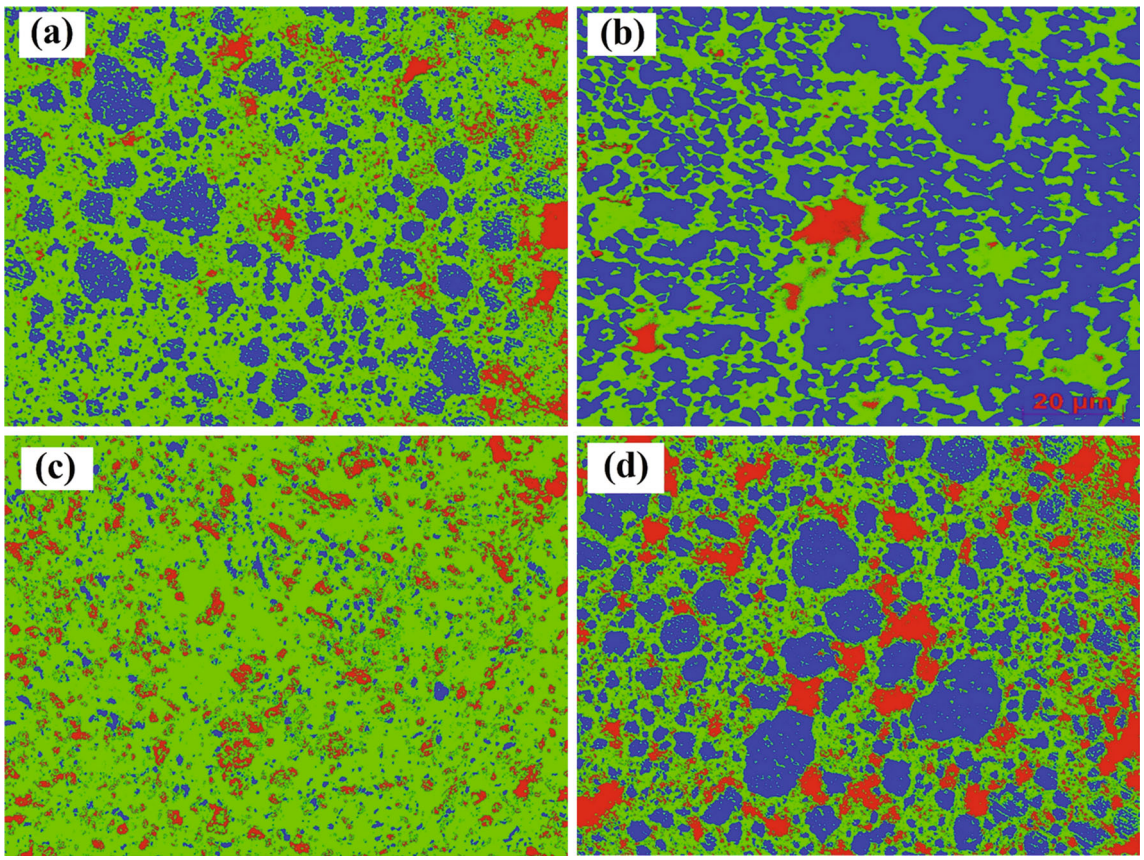

Fig. 10 Phase analysis of duplex **a**, ferritic stainless steel **b**, yttria-dispersed duplex **c** and yttria-dispersed ferritic stainless steel **d** samples sintered at 1000 °C in nitrogen atmosphere (ferrite—*blue*, austenite—*green*, chromium nitride—*red*)

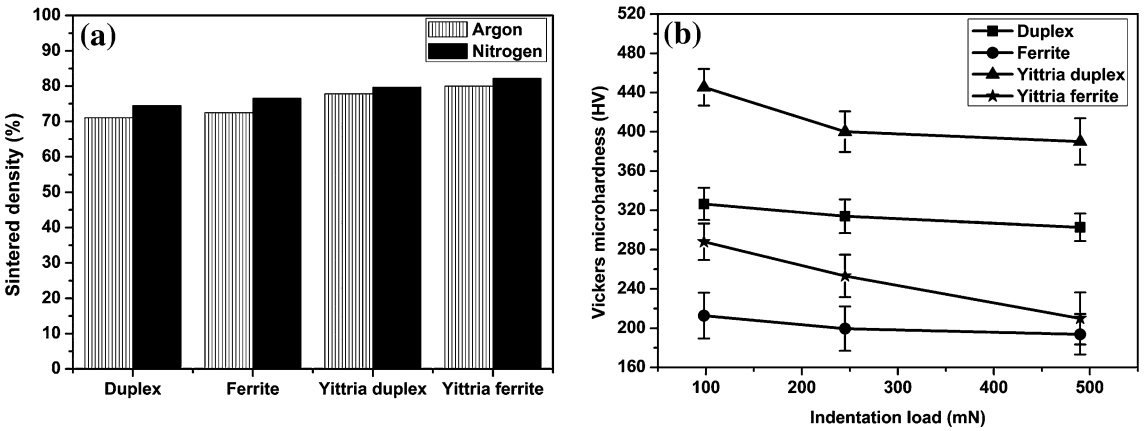

Fig. 11 Curves of sintered density (argon and nitrogen) **a** and Vickers microhardness **b** of stainless steel samples sintered at 1000 °C in nitrogen atmosphere

sintered in argon atmosphere shows maximum porosity and irregular shape and hence less density values. Duplex and ferritic stainless steels sintered in nitrogen atmosphere show densities of 74% and 77%, respectively. Similarly, yttria-dispersed duplex and ferritic stainless steels possess the densities of 80% and 82%, respectively. From Figs. 9 and 10, it is confirmed that the secondary phase such as Cr_2N is formed in all the stainless steel samples sintered under nitrogen atmosphere at 1000 °C. Formation of the secondary phase at the grain boundaries improves the hardness, density and strength of the stainless steel significantly. Figure 11b represents the effect of indentation load

Table 3 Volume fractions, density and hardness of austenite, ferrite and chromium nitride phases of yttria-dispersed and yttria-free stainless steel samples sintered in nitrogen atmosphere at 1000 °C

Sample	Volume fraction (%)			Theoretical density (g/mL)	Sintered density (%)	Vickers microhardness (HV)
	Austenite phase	Ferrite phase	Cr_2N			
Duplex stainless steel	63	28	8	7.84	74	314
Ferritic stainless steel	40	58	2	7.75	77	200
Yttria-dispersed duplex stainless steel	79	7	13	7.80	80	400
Yttria-dispersed ferritic stainless steel	45	35	18	7.70	82	253

on the microhardness of yttria-dispersed and yttria-free duplex and ferritic stainless steels sintered at 1000 °C in nitrogen atmosphere. The Vickers microhardness measurements of stainless steel samples were carried out at 98, 245 and 490 mN indentation load with a dwell time of 10 s. It has been found that the hardness value decreases with the increase in the indentation load due to indentation size effect (ISE). Addition of yttria nanoparticles in stainless steel enhances the bonding strength, and therefore, yttria-dispersed stainless steel shows more density and hardness values. The Vickers microhardness values of duplex and ferritic stainless steels sintered at nitrogen atmosphere are 314 and 200 HV, respectively. Similarly, yttria-dispersed duplex and ferritic stainless steels show microhardness values of 400 and 253 HV, respectively, whereas microhardness values of the duplex and ferritic stainless steels sintered at argon atmosphere are 257 and 192 HV, respectively. Similarly, yttria-dispersed duplex and ferritic stainless steels show microhardness value of 332 and 205 HV, respectively. This increased hardness in nitrogen atmosphere is due to the dissolution of nitrogen into stainless steel samples during sintering. The presence of nitrogen not only increases solid solution strengthening but also increases grain size strengthening [51, 52]. The values of the volume fractions, density and hardness of austenite and ferrite phases of yttria-dispersed and yttria-free stainless steel samples sintered in nitrogen atmosphere are tabulated in Table 3.

4 Conclusions

(1) Yttria-dispersed, yttria-free duplex and ferritic stainless steel samples were fabricated successfully by planetary milling followed by conventional sintering.
(2) The increase in sintering temperature from 1000 to 1400 °C increases the density, hardness and α-Fe to γ-Fe phase transformation of duplex and yttria-dispersed duplex stainless steel.
(3) The hardness increases for duplex from 257 to 567 HV and for yttria-dispersed duplex from 332 to 576 HV with the increase in sintering temperature. Similarly, the hardness increases from 192 to 265 for ferritic stainless steel and from 205 to 341 for yttria-dispersed ferritic stainless steel, respectively.
(4) Compressive yield stresses of yttria-free duplex, ferritic, yttria-dispersed duplex and ferritic stainless steel are 312, 295, 360 and 308 MPa, respectively.
(5) Conventional sintering in nitrogen atmosphere favors α-Fe to γ-Fe phase transformation and increases the density and hardness of stainless steel when compared with sintering in argon atmosphere. The increased hardness is due to the formation of Cr_2N phase.
(6) The hardness of duplex, ferritic, yttria-dispersed duplex and yttria-dispersed ferritic stainless steels is found to be 314, 200, 400 and 253 HV, respectively.

Acknowledgments Financial support for this work from the Council of Scientific & Industrial Research (CSIR), India (Grant No. 22/561/11/EMR II Dated 11.04.2011), is gratefully acknowledged.

References

[1] R. Shashanka, D. Chaira, B.E. Kumara Swamy, Int. J. Sci. Eng. Res. **6**, 1863 (2015)
[2] C. Petterson, S. Fager, *Welding practice for the sandvik duplex stainless steels SAF2304, SAF2205 and SAF2507*, vol. S811 (AB Sandvik Steel, Sweden, 1995), p. 1
[3] W.F. Smith, *Structure and Properties of Engineering Alloys*, 2nd edn. (The University of Michigan, McGraw Hill, 1981)
[4] Y.Q. Wang, B. Yang, J. Han, F. Dong, Y.L. Wang, Pro. Eng. **36**, 88 (2012)
[5] R. Shashanka, D. Chaira, B.E. Kumara Swamy, Int. J. Electrochem. Sci. **10**, 5586 (2015)
[6] H. Miyamoto, T. Mirnaki, S. Hashimoto, Mater. Sci. Eng. A **319**, 779 (2001)
[7] T. Liang, X. Hu, X. Kang, D. Li, Acta Metall. Sin. (Engl. Lett.) **26**, 517 (2013)
[8] L.A. Dobrzanski, Z. Brytan, M. Actis Grande, M. Rosso, Arch. Mater. Sci. Eng. **28**, 217 (2007)
[9] X. Li, J. Shu, L. Chen, H. Bi, Acta Metall. Sin. (Engl. Lett.) **27**, 501 (2014)
[10] C. Suryanarayana, Prog. Mater. Sci. **46**, 1 (2001)
[11] R. Shashanka, D. Chaira, Powder Technol. **259**, 125 (2014)
[12] S. Balaji, A. Upadhyaya, Mater. Chem. Phys. **101**, 310 (2007)
[13] R. Liu, D.Y. Li, J. Mater. Sci. **35**, 633 (2000)

[14] E.J. Felten, J. Electrochem. Soc. **108**, 490 (1961)
[15] C.S. Wukusick, J.F. Collins, Mater. Res. Stand. **4**, 637 (1964)
[16] J.M. Francis, W.H. Whitlow, Corros. Sci. **5**, 701 (1965)
[17] S.L. Li, B.Y. Huang, Y.M. Li, S.Q. Liang, D.X. Li, J.L. Fan, J. Cent. South. Univ. Technol. **10**, 1 (2003)
[18] U. Lindstedt, B. Karlsson, J. Powder Metall. **41**, 261 (1998)
[19] Naci Kurgan, Mater. Des. **52**, 995 (2013)
[20] F. Martin, C. Garcia, Y. Blanco, Mater. Sci. Eng. A **528**, 8500 (2011)
[21] S. Pandya, K.S. Ramakrishna, A.R. Annamalai, A. Upadhyaya, Mater. Sci. Eng. A **556**, 271 (2012)
[22] K. Vijayalakshmi, V. Muthupandi, R. Jayachitra, Mater. Sci. Eng. A **529**, 447 (2011)
[23] R. Shashanka, D. Chaira, Mater. Charact. **99**, 220 (2015)
[24] R. Shashanka, D. Chaira, Powder Technol. **278**, 35 (2015)
[25] S. Gupta, R. Shashanka, D. Chaira, IOP Conf. Ser. Mater. Sci. Eng. **75**, 012033 (2015)
[26] M. Metikos-Hukovic, R. Babic, Z. Grubac, Z. Petrovic, N. Lajci, Corros. Sci. **53**, 2176 (2011)
[27] M. Gojic, A. Nagode, B. Kosec, S. Kozuh, S. Savli, T. Holjevac Grguric, L. Kosec, Eng. Fail. Anal. **18**, 2330 (2011)
[28] R.M. German, *Sintering Theory and Practice* (Wiley, New York, 1996)
[29] K.S. Hwang, R.M. German, F.V. Lenel, Metall. Trans. **18A**, 11 (1987)
[30] R.M. German, Inter. J. Powder Met. **26**, 23 (1990)
[31] S.M. Tiwari, S. Balaji, A. Upadhyaya, Mater. Sci. Eng. A **492**, 60 (2008)
[32] J. Jain, A.M. Kar, A. Upadhyaya, Mater. Lett. **58**, 2037 (2004)
[33] D.Y. Ye, Mater. Chem. Phys. **93**, 495 (2005)
[34] I. Manika, J. Maniks, Acta Mater. **54**, 2049 (2006)
[35] J.H. Gong, J.J. Wu, Z.D. Guan, J. Eur. Ceram. Soc. **9**, 2625 (1999)
[36] H. Buckle, in *The Science of Hardness Testing and Its Research Application*, ed. by J.H. Westbrook, H. Conrad, (ASM, Metal Park, 1973). p. 453
[37] G.M. Pharr, E.G. Herbert, Y. Gao, Annu. Rev. Mater. Res. **40**, 271 (2010)
[38] B.W. Mott, *Microindentation Hardness Testing* (Butterworths, London, 1957)
[39] H. Buckle, Metall. Rev. **4**, 49 (1959)
[40] N. Gane, Proc. R. Soc. Lond. Ser. A **317**, 367 (1970)
[41] G.P. Upit, S.A. Varchenya, The size effect in the hardness of single crystals, in *The Science of Hardness Testing and Its Research Applications*, vol. 10, ed. by J.H. Westbrook, H. Conrad (ASM, Metals Park, 1973), p. 135
[42] C.C. Chen, A.A. Hendrickson, Microhardness phenomena in silver, in *The Science of Hardness Testing and Its Research Applications*, vol. 21, ed. by J.H. Westbrook, H. Conrad (ASM, Metals Park, 1973), p. 274
[43] S. Pasebani, A.K. Dutt, J. Burns, I. Charit, R.S. Mishra, Mater. Sci. Eng. A **630**, 155 (2015)
[44] S. Qu, C.X. Huang, Y.L. Gao, G. Yang, S.D. Wu, Q.S. Zang, Z.F. Zhang, Mater. Sci. Eng. A **475**, 207 (2008)
[45] E. Salahinejad, R. Amini, M. Marasi, M.J. Hadianfard, Mater. Des. **31**, 527 (2010)
[46] E. Salahinejad, R. Amini, M.J. Hadianfard, Mater. Sci. Eng. A **527**, 5522 (2010)
[47] A. Yadollahi, N. Shamsaei, S.M. Thompson, D.W. Seely, Mater. Sci. Eng. A **644**, 171 (2015)
[48] M. Javanbakht, M.J. Hadianfard, E. Salahinejad, J. Alloys Compd. **624**, 17 (2015)
[49] F. Tehrani, M.H. Abbasi, M.A. Golozar, M. Panjepour, Mater. Sci. Eng. A **528**, 3961 (2011)
[50] R. Mariappan, S. Kumaran, T. Srinivasa, Rao. Mater. Sci. Eng. A **517**, 328 (2009)
[51] J. Abenojar, F. Velasco, A. Bautista, M. Campos, J.A. Bas, J.M. Torralba, Compos. Sci. Technol. **63**, 69 (2003)
[52] E. Salahinejad, R. Amini, M.J. Hadianfard, Mater. Des. **31**, 2241 (2010)